Direct Numerical Simulation of a Spatially Evolving Flow from an Asymmetric Wake to a Mixing Layer

Sylvain Laizet and Eric Lamballais

Laboratoire d'Etudes Aérodynamiques UMR 6609, Université de Poitiers, CNRS
Téléport 2 - Bd. Marie et Pierre Curie B.P. 30179
86962 Futuroscope Chasseneuil Cedex, France
lamballais@univ-poitiers.fr

Summary. In this paper, the flow obtained behind a trailing edge separating two streams of different velocities is studied by means of direct numerical simulation. The influence of the shape of the trailing edge, that can be either blunt or bevelled, is considered through the analysis of the destabilizing mechanisms and their resulting effects on the spatial development of the flow. It is shown that the use of a bevelled trailing edge leads to a conventional mixing-layer dynamics with moderate effects of the wake component. In contrast, a self-excited flow is obtained behind a blunt trailing edge where usual features of the wake dynamics are recovered. In terms of receptivity, it is found that the flow behind a bevelled trailing edge is strongly sensitive to upstream perturbations. The inverse behaviour is observed for the flow behind a blunt trailing edge. These differences are interpreted in terms of convective/absolute stability. The vortical organization obtained in each case is discussed using vorticity visualization.

1 Introduction

It is well known that the spatial development of turbulent wakes or mixing layers is strongly influenced by the dynamics of large scale vortices. For a wake flow, the alternating large structures (called Karman vortices) are initially created through a vortex shedding mechanism occurring immediately behind the body considered. For a mixing layer flow, the formation of primary structures leads to co-rotating Kelvin-Helmholtz vortices. In terms of stability, the mechanisms responsible of these two vortex families are of different nature. In typical wake flows, the vortex shedding is a self-excited phenomenon that can be interpreted in terms of global instability [7]. In contrast, Kelvin-Helmholtz formation in spatial mixing layers admits a strong sensitivity to upstream conditions as a consequence of the convectively unstable character of this type of flow.

In many applications, the flow over a given geometry leads to an asymmetric wake that can be viewed as a flow with a double component wake/mixing-layer.

Compared to a conventional wake, a strong breaking in the symmetry can change deeply the spatial development of the flow. The same can be said by comparison with a pure mixing-layer, the wake component being able to introduce very different mechanisms in the vortex generation behind the geometry. In order to investigate the dynamics of this type of hybrid flow, we consider here the general flow configuration where two independent streams of velocity U_1 and U_2 are flowing on opposite sides of a semi-infinite plate of thickness h (see figure 1 for a sketch of the flow geometry). The asymmetry of the flow can be quantified through the dimensionless parameter $\lambda = \frac{U_1 - U_2}{U_1 + U_2}$ defined as usually for a conventional spatial mixing layer. Just behind the trailing edge, a wake takes place while further downstream, the decreasing velocity deficit can lead the flow to transition from a wake regime to a mixing layer regime. The persistence of the wake is naturally dependent on the asymmetry parameter λ but also on the more of less marked of the wake component that can be linked to the shape of the trailing edge.

An experimental investigation of the case $\lambda = 0.2$ was carried out by [3] who have compared the flow obtained with a bevelled trailing edge with the one generated downstream a thick splitter plate (blunt trailing edge). In the first case, a Conventional Mixing Layer was observed (CML case) while in the second one, a composite wake/mixing-layer flow was noticed and designated as a Thick Mixing Layer (TML case). The goal of the present numerical study is to investigate by DNS a flow configuration similar to the experimental set-up of [3] in order to better understand the reasons of the deep changes introduced by the shape of the trailing edge, in the vicinity of the trailing edge as well as further downstream. An improvement of the understanding of these fundamental mechanisms should be helpful in the context of flow control via the passive or active modification of trailing edge geometry.

2 Numerical methods and computational flow configuration

A numerical code fully based on sixth-order compact finite difference schemes and a Cartesian grid is used to solve the incompressible Navier-Stokes equations. The incompressibility condition is ensured via a fractional step method introducing a Poisson equation for the pressure. An original characteristic of the present code, called "Incompact3d", is that this equation is directly solved in the framework of the modified spectral formalism. More precisely, our Poisson solver is only based on 3D Fast Fourier Transforms (FFT3D) despite the use of inflow/outflow boundary conditions. This very direct solving technique is obviously possible for periodic and free-slip boundary conditions, but also when Dirichlet conditions for the velocity are combined with homogeneous Neumann conditions for the pressure (see for instance [14], [12] for the basic principles of the spectral solving of a Poisson equation based on cosine expansion). Note that homogeneous Neumann conditions provide only second order accuracy in the corresponding direction, even if high-order finite difference schemes are used. This formal drawback is considered here as being of secondary importance, the excellent behaviour of our sixth-order schemes being preserved outside from the near inflow/outflow regions. In addition, the full spectral treatment of Poisson equation offers three major advantages: (i) it allows the very easy staggering of the grid pressure; (ii) it allows the introduction of a grid stretching in one

direction by preserving the direct nature of the solver ([4], [1]); (iii) its cost can be less than 10% of the overall computational expense (for regular and collocated grids) while never overtaking 20% (for stretched and staggered grids). Concerning the former point, we follow here our recent conclusions of a previous work [8] by using staggered pressure grid in order to avoid the excitation of pressure oscillations due to the immersed boundary treatment. More details about the present computational methodology can be found in this study [8].

The trailing edge is modelled using an immersed boundary technique where the specific direct forcing method of [11] is employed. Basically, the principle of this method is to calibrate the forcing in order to verify the no-slip condition at the wall of the body while trying to ensure the regularity of the velocity field across the immersed surface by creating an artificial flow (with a mass source/sink) inside the body. This particular procedure was found to improve significantly the results when high-order schemes are used for the spatial differentiation (see [11] for more details).

The governing equations are directly solved in a computational domain $L_x \times L_y \times L_z = 63h \times 96h \times 9h$ discretized on a Cartesian grid of $n_x \times n_y \times n_z = 561 \times 257 \times 80$ points except for 2D simulation where $n_z = 1$. The stretching of the grid in y-direction leads to a minimal mesh size of $\Delta y_{\min} \approx 0.03h$. Inflow/outflow, free-slip and periodic boundary conditions are used in x, y and z directions respectively. The geometry parameters correspond to the experimental conditions of [3] concerning the shape of the trailing edges (see figure 1), the boundary layers thicknesses $\delta_1 = 0.57h$ and $\delta_2 = 0.50h$ and the velocity ratio $\lambda = 0.2$. Present DNS show two significant differences with respect to experiments. First, the Reynolds number $Re = \frac{(U_1 - U_2)h}{\nu}$ is reduced from 14400 to 400, and secondly, both inflow boundary layers are laminar (mean Blasius-like profiles) whereas they are turbulent in experiments. Consequently, only a qualitative agreement with experiments can be expected.

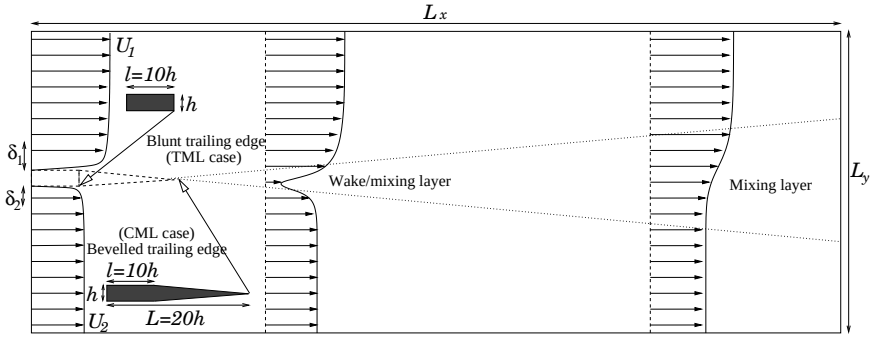

Fig. 1. Flow configuration and computational domain.

3 Preliminary 2D simulations

Despite their artificial nature, 2D DNS performed without any inflow perturbation can be instructive in terms global stability characteristics for each case (CML or TML). The resulting flows are illustrated in figure (2ac). Both flow configurations lead to a quasi-steady behaviour where vortices are formed periodically and convected downstream. These established states are obtained after a transient stage where the computed flow has to adapt to initial conditions and to evacuate them. By performing several DNS based on various initial conditions (strongly, weakly or not at all perturbed), we verified that both flows can forget their initial conditions and finally reach the steady-periodic behaviour illustrated in figure (2abcd). In the TML case, a vortex shedding can be clearly identified through the presence of co- and counter rotating vortices in the near-edge region while for the CML case, only vortices of negative spanwise vorticity ($\omega_z < 0$) are created significantly further downstream. In first analysis, the behaviour of the TML case seems to be related to a globally unstable situation leading to a self-excited dynamics. More precisely, both blunt and bevelled trailing edges introduce a velocity deficit and a near-wake region that is absolutely unstable in a local analysis. However, it can be expected that the resulting pocket of absolute instability is clearly more reduced in the CML than for the TML case, in such a way that no global modes can exist in the former case.

The same 2D DNS were performed again using inflow perturbations correlated in time and space. By the term correlated, we mean that the noise used to define inflow perturbations is not purely white (non-correlated data) while being of large band-width in the spectral space. This type of inflow treatment was previously shown to improve the realistic character of a spatial flow in the inlet region. Using these inflow conditions, more realistic results are obtained for the CML case

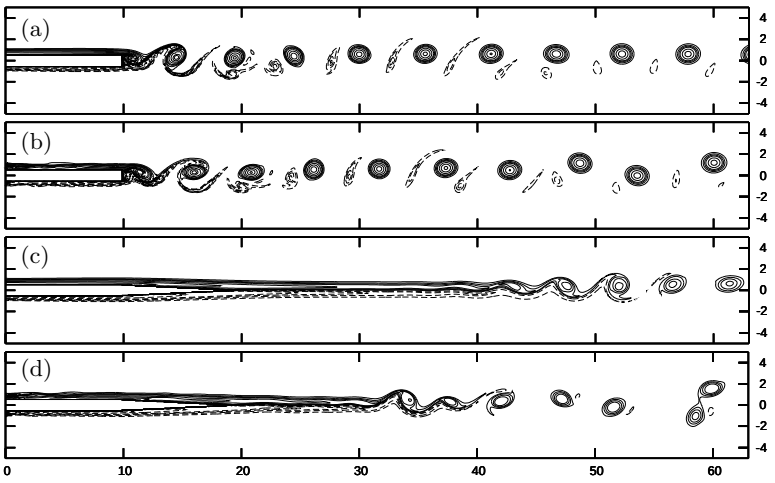

Fig. 2. Vorticity contours for DNS 2D results (dashed lines indicate positive contours). TML (ab) and CML (cd) cases with (bd) or without (ac) inflow perturbations.

whereas minor modifications are obtained for the TML case (see figure 2cd). The main improvement concerns the location of the primary Kelvin-Helmholtz that can appear more upstream in agreement with experimental observations. The main frequency f associated to the primary (Kelvin-Helmholtz or Karman) vortex passing lead to $St = 0.17$ for the TML case and $St = 0.21$ for the CML case, where St is the Strouhal number defined by $St = fh/U_c$. The Strouhal number obtained for the TML case is consistent with [6] who found $St \approx 0.11$ at $Re = 128$ while highest values $0.2 \leq St \leq 0.24$ are found for significantly higher Reynolds numbers [2, 3]. Concerning the global overall of the TML flow, in agreement with previous observations of [6, 3], a shifting of the mixing layer centre towards the high velocity region is well recovered in present results (see figure 2ab), whereas the inverse tendency occurs very slightly for the CML case.

Finally, it seems possible to conclude from these DNS 2D that the wake component is strongly dominated by the mixing-layer component everywhere in the CML flow, where primary and secondary (pairing) instability phenomena can be clearly observed as it can be expected for a conventional mixing layer. In contrast, both components play a various role in the TML case depending on the x-location. In the near-edge region, a typical wake behaviour can be observed while further downstream, vortices of positive vorticity are progressively damped, the Karman street becoming gradually asymmetric and leading finally (for $x > 40h$) to a spatial mixing-layer flow. This downstream evolution for an asymmetric wake to a mixing-layer is consistent with the previous DNS of [6]. These behaviours will be discussed more in detail in the next section by considering a more realistic flow configuration.

4 Results of 3D simulations

In this section, 3D DNS of TML and CML cases are presented and compared to the experimental results of [3]. Both calculations use exactly the same perturbed inflow data. For these two simulations, a fully 3D dynamics is obtained with the presence of large scale coherent structures. For the CML case, in a similar way than in the previous section, no wake component can be identified qualitatively in the vortex dynamics observed via animations. An illustration of the flow is presented in figure 3cd through vorticity visualizations. The formation of Kelvin-Helmholtz vortices submitted to parings further downstream can be easily identified.

A similar main frequency is obtained for the primary instability with $St = 0.22$. Moreover, it can observed that 3D motions are in qualitative agreement with reference studies on the spatial mixing layer (see for instance [5]) where the typical flow topology involving longitudinal structures stretched between large spanwise rolls is well recovered here. Despite the fully 3D nature of the development of the flow, no self similar turbulent state can be expected, the present computational domain being to short in the x-direction. This view is clearly confirmed by the analysis of turbulent statistics (non presented results) that clearly shows the signature of a transitional mixing layer where the vertical/spanwise velocity fluctuations are over/under-predicted respectively by comparison with self-similar turbulent mixing-layer results.

The preliminary observation of vorticity visualisations (see figure 3ab) obtained in TML case suggests clearly that the mechanisms associated to the self-excitation of the flow allows the reaching of a highly 3D turbulent state immediately behind

the blunt trailing edge. In first analysis, this behaviour is consistent with the experimental observations of [3] who also have detected the occurrence of vortex shedding in the near trailing-edge region (see figure 4 for a visual comparison between experimental and DNS visualisations covering an identical sub-domain).

The tendencies already observed in DNS 2D results are recovered here, especially the deviation of the layer towards the high velocity region and the strongly marked wake dynamics that evolves progressively towards a mixing-layer dynamics. This change of regime associated to the spatial development of the flow can be identified qualitatively by observing the gradual disappearance of large scale spanwise structure in the slow part of the flow. Downstream from $x \approx 40h$, only big rolls of negative vorticity (i.e. of the same sign than the vorticity associated to the mixing layer velocity profile) can be visually detected in animations. Despite the lack of any wake signature in the vortical organization of the flow for $x > 40h$, the spatial development of the flow does not correspond to the one expected for a mixing layer. The more drastic change concerns the pairing that can never be observed for the present TML case, this tendency being already present in 2D DNS results.

It is well known that pairings contribute strongly to the expansion of a mixing layer. Here, in the absence of any paring, we find a spreading rate $d\delta/dx \approx 0.024$ significantly weaker than for a conventional mixing layer. This behaviour is in complete contradiction with the experimental results of [3] who find an important increase of the TML expansion compared with the CML one, the growth rate being almost doubled when a blunt trailing edge is used. The consequence of this difference can be directly observed by comparison between mean velocity profiles obtained experimentally and computationally at the same location $x = 42h$ (see figure 5), the mixing layer thickness being underestimated by a factor 2 in present DNS.

We cannot propose any simple explanation of this disagreement between experiments and present calculations. The main difference between present DNS and experiments concerns the Reynolds number and the inflow conditions that are not

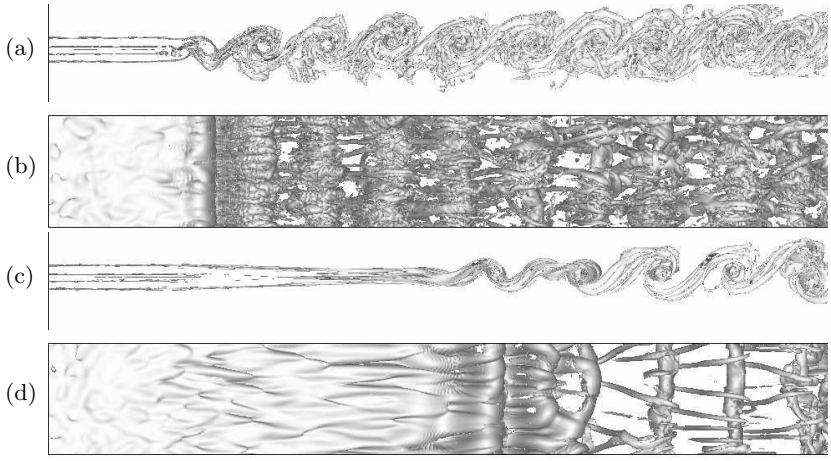

Fig. 3. Vorticity isosurfaces for DNS 3D results. TML (top) and CML (bottom) cases in side or upper views.

realistic enough here to allow the establishment of self-similar conditions as quickly as in experiments. Therefore, more investigations seem to be required by considering the influence of the Reynolds number using LES [9], the impact of the use of realistic inflow conditions (that can be based on DNS/LES data of turbulent boundary layers using the technique of [10]) or the effects of the size of the computational domain in z-direction[1].

Naturally, the poor agreement between present DNS and experiments concerning the growth rate of the TML is recovered in other turbulent statistics like Reynolds stresses (non presented results), the main difference being that DNS leads to a more 2D flow than the one reported in experiments, the more spectacular consequence of this tendency being the overestimation of transverse velocity fluctuations that are more than twice stronger in DNS compared with measurements.

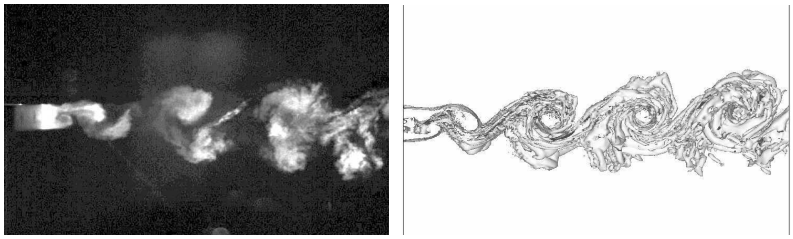

Fig. 4. Experimental (left, [3]) and vorticity (right, present DNS) visualizations of the TML.

To end this section, let us consider the velocity deficit associated to the wake component in the TML case. The spatial stability characteristics of a generic composite mixing-layer/wake profile $U(y)/U_m = 1 - f\,\mathrm{sech}^2(y/\delta) + \lambda\tanh(y/\delta)$ has been considered by [13]. For the present velocity ratio $\lambda = 0.2$, [13] have shown that if $f > 0.95$, the corresponding flow become absolutely unstable. For present DNS results, it is worth noting that the mean velocity profile can be very well fitted (via the relevant adjusting of δ) by the generic profile of [13] in the near trailing edge region (see figure 5). Moreover, the wake deficit parameter can be evaluated from the mean velocity field in each x-location through the relation $f(x) = (U_m - \min_y[\langle u\rangle(x,y)])/U_m$. The longitudinal evolution of this parameter is presented in figure 5. An acceptable agreement is found between DNS and experiments. For present results, using the criterion $f > 0.95$, the region $0 < x - l < 1.6h$ is found to be absolutely unstable. Note that if the same procedure is repeated for the CML (non-presented curve), the absolutely unstable zone of the flow is found to be significantly smaller, the condition being $0 < x - L < 0.2h$ in this case. This change of the size of the pocket of absolute instability, depending of the shape of the trailing edge, suggests once again that the TML flow is globally unstable (leading to self-excitation) contrary to the CML flow.

[1] We have considered the influence of the spanwise length L_z by increasing its value by 50% (while keeping constant the mesh size) but we did not see any significant effect on the results discussed here for both TML and CML cases.

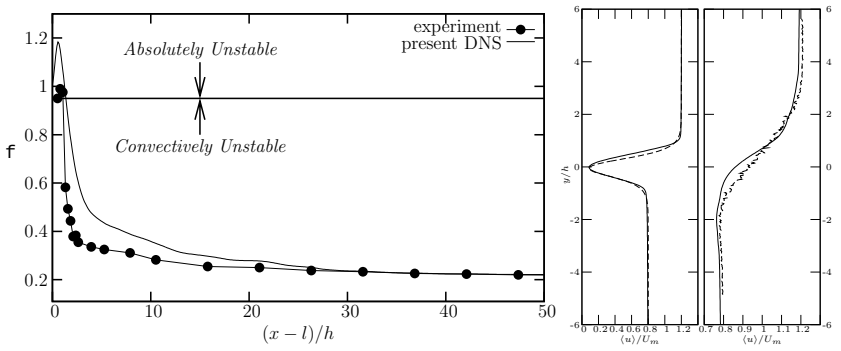

Fig. 5. Left: Longitudinal evolution of the wake deficit parameter $f(x) = (U_m - \min_y[\langle u \rangle(x,y)])/U_m$. Centre: Comparison of the mean velocity profile at $x - l = 1.6h$ (solid line) with the generic profile used by [13] (dotted line). Right: Comparison of the mean velocity profile at $x - l = 42h$ (solid line) with its experimental counterpart [3].

Acknowledgments: Calculations were carried out at the IDRIS. We are grateful to Jalel Chergui, Jean-Marie Teuler and Laurent Perret for their precious help.

References

1. E.J. Avital, N.D. Sandham, and K.H. Luo. *Int. J. Numer. Methods Fluids*, 33:897–918, 2000.
2. D. R. Boldman, P. F. Brinich, and M. E. Goldstein. *J. Fluid Mech.*, **75**:721–735, 1976.
3. C. Braud, D. Heitz, G. Arroyo, L. Perret, J. Delville, and J.-P. Bonnet. *Int. J. Heat and Fluid Flow*, 25(3):351–363, 2004.
4. A.B. Cain, J.H. Ferziger, and W.C. Reynolds. *J. Comp. Phys.*, 56:272–286, 1984.
5. P. Comte, J.H. Silvestrini, and P. Bégou. *Eur. J. Mech. B/Fluids*, **17**(4):615–637, 1998.
6. D. A. Hammond and L. G. Redekopp. *J. Fluid Mech.*, **331**:231–260, 1997.
7. P. Huerre and P. A. Monkewitz. *Ann. Rev. Fluid Mech.*, **22**:473–537, 1990.
8. S. Laizet and E. Lamballais. In *Proc. IV Escola de Primavera de Transiçao e Turbulência*, Porto Alegre, RS, Brazil, 2004.
9. M. Lesieur, O. Métais, and Pierre Comte. *Large-eddy simulation of turbulence*. Cambridge University Press, 2005.
10. T. S. Lund, X. Wu, and K. D. Squires. *J. Comp. Phys.*, **140**:233, 1998.
11. P. Parnaudeau, E. Lamballais, D. Heitz, and J. H. Silvestrini. In *Proc. DLES-5*, Munich, 2003.
12. P. N. Swarztrauber. *SIAM Review*, **19**:490–501, 1977.
13. D. Wallace and L. G. Redekopp. *Phys. Fluids*, **4**(1):189–191, 1992.
14. R. B. Wilhelmson and J. H. Ericksen. *J. Comp. Phys.*, **25**:319–331, 1977.